JOURNAL OF MATERIALS SCIENCE 11 (1976) 150–163

The effect of oxide surface layers on the breakdown voltage in metal-vacuum-metal sandwiches

ASHOK K. VIJH
Institut de Recherche de l'Hydro-Québec, C.P. 1000, Varennes, Québec, JOL 2PO, Canada

K. DIMOFF
INRS-Energie, Université du Québec, C.P. 1020, Varennes, Québec, JOL 2PO, Canada

Correlations are explored between the observed breakdown voltages in metal–vacuum–sandwiches and the properties of the metallic electrodes which are believed to be covered by oxide layers. A linear relationship is indicated between the work function of the electrode and the breakdown voltage. This relationship may prove useful in obtaining more accurate estimates for the breakdown voltage of the vacuum dielectric itself, when it is sandwiched between a wide variety of electrode materials.

1. Introduction

Allan and Salim [1] have issued recent data concerning the relation between pre-breakdown currents and the breakdown voltage for various metal–vacuum–metal sandwiches. The dependence of breakdown voltage on interelectrode separation and the temperature (4.2, 77.3 and 300 K) was explored.

Their results were presented in terms of Fowler–Nordheim (F–N) plots [1, 2]. It was found that the F–N emission theory [2, 3] governed the current flow in the gap up to breakdown, but that deviations occurred upon breakdown. Variations in breakdown voltage were attributed to changes in the field intensification factor and the effect of contamination layers. Under the experimental conditions, the electrode materials used by Allan and Salim [1] were invariably covered by oxides (Al, Cu, Nb, stainless steel) with the possible exception of Au. However, no attempt was made by them to relate the effects of the presence of oxides on metals with observed breakdown voltages in a quantitative way.

The influence of oxide layers, contaminating films and gases desorbed from electrode and/or discharge vessel surfaces upon current-voltage characteristics of the vacuum arc under pre-breakdown and breakdown conditions have been subjects of concern in many studies. In an attempt to reconcile observed surface conditions for a tungsten cathode with the requirements of local field enhancement, Walters *et al.* [4] have included in their calculations an electrode oxide film > 100 Å thick, as well as an additional overlayer $\geqslant 70$ Å in depth of carbon-based contamination. Latham [5] and Fane *et al.* [6] have measured the growth of equilibrium thicknesses of oxide film at standard temperature and pressure on copper (~ 20 Å) and stainless steel (30 to 50 Å). They also demonstrate that a temperature in excess of 1300 K is required to remove such a deposit of stainless steel oxide at 10^{-8} Torr. Thus adequate preconditioning of the electrodes in vacuum ($< 10^{-8}$ Torr) is essential to ensure complete removal of electrode surface contamination and the possibility of oxide film formation.

In addition, Beukema [7] has demonstrated that ions, released from adsorbed gas layers on the anode by field emission electrons, can change the emitting properties of a well-conditioned cathode. Further evidence of the role played by anode material properties on the breakdown characteristics of the gap, and by inference their effect on the emitting characteristics of the cathode, has been

shown by Rosanova and Granovskii [8].

Adams and Germer [9] explore the change in work function of an electrode surface with the adsorption of CO at room temperature. Moreover, Denholm [10] demonstrates the possible effect that pump vapour, a prime source of CO and carbon-based contamination, can have on the breakdown voltage of a vacuum gap.

In all cases, attempts are made to stabilize pre-breakdown currents or breakdown voltages either by repetitive sparking [11-13] or by a d.c. current applied in vacuum [1] and/or in a hydrogen environment [10, 14]. Such preconditioning procedures do not necessarily preclude the formation of metallic oxide film on those parts of the cathode surface which control the pre-breakdown or breakdown phenomenon under study.

Traces of oxygen are always present in the vacuum gap, as well as adsorbed on the electrode material. Oxygen can also be liberated by the decomposition of carbon-based contaminant at high temperatures during the preconditioning process or upon breakdown. The presence of metallic vapour ions or excited atoms emanating from the anode under electron bombardment would therefore favour the formation of oxides near the relatively cold cathode surface. Direct transfer of metallic oxide from anode to cathode can also occur under discharge conditions. The effective electrode area which controls the discharge is quite small [15] so that the presence of only minute traces of oxide in vapour form can lead to the buildup of oxide layers sufficiently thick to dominate the emission characteristics of the cathode surface.

Although the presence of contaminants and oxides has been mentioned by the authors quoted above, the effects of these materials on the breakdown voltage in metal–vacuum–metal sandwiches have been dealt with only in a qualitative manner. An attempt at a quantitative analysis is undertaken in this article, based on the recent work of Trasatti [16] and Johnson [17] in connection with the surface work functions of metals and their change due to the presence of oxygen. For simplicity, and because of the tendency towards oxide formation by metallic electrodes as discussed above, only the oxide surface characteristics of the relevant metals will be investigated.

Moreover, since the primary experimental evidence [1] upon which this article is based deals mainly with gap separations $\delta \leqslant 1$ mm, the appellation "sandwich" is meant to designate submillimetre gaps.

Parenthetically, it should be noted that although the formation of an oxide on Au is unlikely on thermodynamic grounds, such a process is quite possible due to *kinetic* considerations under the experimental conditions used by Allan and Salim [1]. An example of the latter possibility occurs during the heating of Au in air, or when anodic electric fields are present at either metal–gas or metal–electrolyte interfaces [18]. One must therefore assume the presence of an oxide layer, howsoever thin, even on Au. This assumption is further reinforced by the fact that the parameters upon which the F–N theory depends (such as local electric field strengths, intensification factors, work functions, etc.) are influenced strongly by the state, preparation and conditioning of the surface.

An important influence on the magnitude of the breakdown voltage, at a given temperature and metal–(vacuum)–metal spacing, is the relevant property or properties of the electrode material. Hence the actual condition of the electrode surface, namely the oxide coating, must be taken into account in the analysis of data concerning voltage breakdown. The purpose of this article is to delineate some properties of oxide-coated electrodes that show a direct relation to the magnitude of voltage breakdown V_b at a given temperature and electrode separation, δ.

At all temperatures below 300 K, V_b versus δ plots exhibit the same general trends ([1] Figs. 4 and 5). It should therefore be sufficient to illustrate the oxide effect with data pertaining to one temperature only, namely 300 K.

2. Correlation between oxide band gap and the breakdown voltage

The possible influence of semiconductivity effects, characteristic of the oxide covering the electrode, upon the breakdown voltage V_b is best illustrated by plotting V_b values for various electrode materials against the band gap, E_g, of their corresponding oxides.

Since an E_g value for the oxide of Au is not available, the matter may be explored by using the heat of formation per equivalent, ΔH_e, values of the oxides under study. This can be done since, for a large number of inorganic compound semiconductor [19],

$$E_g \simeq 2(-\Delta H_e). \qquad (1)$$

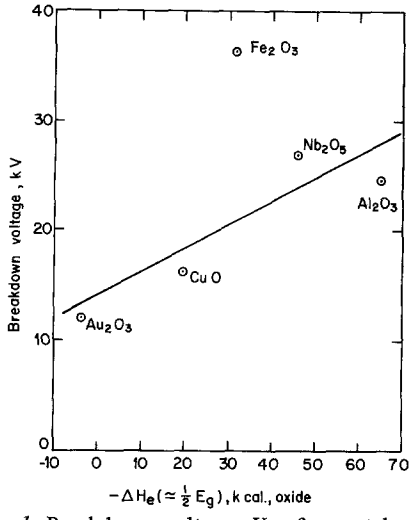

Figure 1 Breakdown voltage, V_b, for metal–vacuum–metal sandwiches composed of indicated metals versus heat of formation per equivalent, $-\Delta H_e$, (or half band gap) of the corresponding metallic oxide. (Data from Table I.)

Fig. 1 demonstrates that V_b increases with increasing $-\Delta H_e(-\frac{1}{2}Eg)$ for the pure metal oxides of Au, Cu, Nb, Al. Stainless steel (designated by Fe in Fig. 1) departs from the general trend since Equation 1 only applies to oxides formed by pure metals. Table I summarizes the data underlying Fig. 1, together with the appropriate reference sources.

The linear trend in Fig. 1 suggests that the observed V_b must contain a component corresponding to a potential drop across the semiconducting oxide. In the case of highly insulating oxides, such as those of Nb and Al, there is an appreciable potential drop across the oxide layer. Hence the measured V_b value consists of a component pertaining to the breakdown of the vacuum dielectric and another component arising from the potential drop across the semiconducting oxide layer covering the electrode. Conversely, the oxides of Au and Cu are highly conducting (in comparison to those of Nb and Al), so that lower potential drops occur across the oxide layer and thereby lower overall V_b values.

In the case of stainless steel it is possible that the surface oxide is predominantly chromium rather than that of iron [6, 20]. However, the heat of formation per equivalent, ΔH_e, of iron oxide used in this analysis (Table I, Fig. 1) lies within the range of this property for the chromium oxides [21, 22]:

$$\begin{aligned}\Delta H_e(Cr_2O_3) &= -45 < \Delta H_e(Fe_2O_3) \\ &= -36.5 < \Delta H_e(CrO_3) \\ &= -23.1 \text{ kcal} \end{aligned} \quad (2)$$

From Equation 1 it can be seen that the semi-

TABLE I Breakdown voltages for metal–vacuum–metal sandwiches and appropriate quantities of the corresponding electrode material.

(a)	(b)	(c)	(d)	(e)	(f)	(g)	
Metal	ϕ_M (eV)	V_b (kV)	$-\Delta H_e$ (kcal)	$\Delta\phi_0$ (eV)	ϕ_{MO} (eV)	T_{MO} (°C)	T_M (°C)
Al	4.19	24.5	65	2.0	6.19	2027	660
Cu	4.70	16.0	20	0.68	5.38	1336	1083
Nb	4.20	27.0	46	1.90	6.1	1512	3000
Au	4.78	12.0	−3.5	0.90	5.68	<500	1063
Fe* or Stainless steel	4.65*	36.5	32*	1.84*	6.49*	1597*	1530*

(a) The tabulated metals are those used in metal–vacuum–metal sandwiches studied by Allan and Salim [1].
(b) The most reliable and recent values for the work function of pure, bare metals, ϕ_M, as given by Trasatti [16].
(c) Observed values of the breakdown voltage, V_b, at 300 K and 0.4 mm electrode spacing as reported in [1]: Figs. 4 and 5.
(d) Heat of formation per equivalent, ΔH_e, values for the oxides of the corresponding metal from Sanderson [21]; the band gap $E_g \simeq 2(-\Delta H_e)$ as discussed in [19].
(e) $\Delta\phi_0$ refers to the increase in the work function of the metal, observed experimentally (except for Al and Fe), due to the formation of a layer of chemisorbed oxygen on the metal; after Johnson [17]. The value for Al is estimated from comparison with the closely related cases for Ta, Nb and Ti; the value of $\Delta\phi_0$ for Fe is the calculated one [17].
(f) The work function of the oxide-covered metal $\phi_{MO} = \phi_M + \Delta\phi_0$.
(g) T_{MO}, melting point of the oxide [27]; T_M, melting point of pure metal [51].

* Quantities for pure iron, since ϕ_M, $-\Delta H_e$ and $\Delta\phi_0$ values for stainless steel are not available.

conductivity of the oxides for Fe and Cr are comparable. Hence the correlation point for stainless steel (Fe) in Fig. 1 remains distinctly apart from the main trend exhibited by the other materials under study.

The position of Au in Fig. 1 can be taken as the limiting case in which the potential drop across the oxide is negligible, since one would expect gold oxide to be highly conducting. The observed V_b value for the Au–vacuum–Au sandwich may therefore be regarded as representative of breakdown of the dielectric (in the metal–vacuum–metal sandwich) itself for a given temperature and electrode spacing.

3. Correlations between work functions of oxide-covered metals and the breakdown voltage

3.1. The Fowler–Nordheim relation

The Fowler–Nordheim (F–N) equation for field emission from an electrode into vacuum may be written as [23]:

$$j = I/A = K_1 F^2 \phi^{-1} \exp[-K_2 \phi^{3/2}/F] \quad (3)$$

where j is the current density, I the total current in amps, A the effective emitting area of the electrode (cathode) in m^2, F the enhanced electric field at the cathode in Vm^{-2} and ϕ is the work function of the emitting surface in eV. The derivation of Equation 3 is available in [2a, 24, 25], while the temperature dependent version is given in [3].

The coefficients of Equation 2 are:

$$K_1 = 1.54 \times 10^{-6}, \quad K_2 = 6.83 \times 10^9 v(y) \quad (4a)$$

where

$$y = 3.79 \times 10^{-5} F^{1/2}/\phi \quad (4b)$$

as shown in [14, 15, 26] with tabulated values of the slowly varying function $v(y)$ presented in [25, 27].

The enhanced electric field at the emitting surface is:

$$F = \beta E = \beta |V|/d \quad (5)$$

where E is the average field arising from an external voltage of V volts which is applied across a gap separation of d meters (to be regarded as distinct from the millimeter notation $\delta = 10^{-3} d$). The geometric significance of the field intensification factor β is outlined in [15, 26, 28]. References [14, 25] demonstrate the method of measuring β from F–N plots, where the slope γ is defined by:

$$\gamma = \frac{6.83 \times 10^9 \phi^{3/2}}{\beta} S(y) \quad (6)$$

and $S(y)$ is another slowly varying function which is also tabulated in [25, 27].

Provided the current–voltage characteristics of the gap are controlled primarily by emission processes up until breakdown (j_b, I_b, V_b), then from Equations 3, 4a, b and 5), the relation:

$$\ln(\phi/V_b^2) = K_3(\phi^{3/2}/V_b) \quad (7)$$

with K_3 a constant, should hold for the various materials under study at the same gap separation δ and cathode temperature [1].

The validity of Equation 7 implies that the field intensification factors β at breakdown of the various electrode surfaces remain similar in magnitude. Of equal importance is the requirement that breakdown current densities j_b for the different metal–vacuum–metal sandwiches vary no more than an order or two in magnitude.

In keeping with the discussion of the previous sections, it is to be understood that the work function of the emitting surface is not that of the bare metal ϕ_M, but of the oxide-covered metal ϕ_{MO}. Fig. 2 verifies that the linear relationship in Equation 7 between $\ln(\phi_{MO}/V_b^2)$ and $(\phi_{MO}^{3/2}/V_b)$ does exist for oxide-covered electrodes. As suggested in the previous section, the contribution of oxides in the Au case can be regarded as negligible.

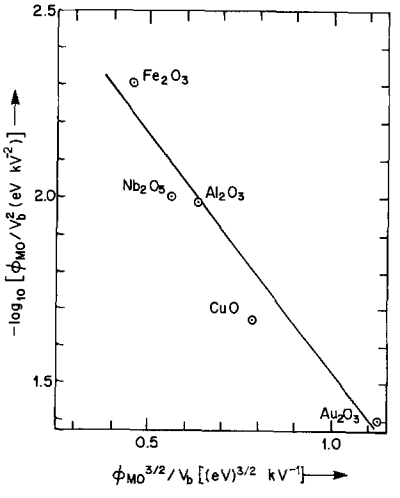

Figure 2 Fowler–Nordheim plot including the dependence on work function for oxide-covered metallic electrodes. (Data from Table I.)

TABLE II Surface and breakdown parameters of pure and oxide covered metallic electrodes

(a) Surface	(b) ϕ (eV)	(c) β	(d) V_b (kV)	(e) F_b (10^9 V m^{-1})	(f) F_s (10^9 V m^{-1})	(g) I_b (10^{-4} A)	(h) A (10^{-18} m^2)	(i) j_b (A m^{-2})
$\delta = 0.1$ mm								
Fe	4.65	92	10.5	9.67	8.02	9.3	6.52	1.48×10^{12}
Fe_2O_3	6.49	153		16.1	13.2		6.04	
Al	4.19	169	7.8	13.2	6.9	1.43	2.17	7.49×10^{13}
Al_2O_3	6.19	309		24.1	12.3		1.68	
Au	4.78	386	4.5	17.4	8.4	1.95	0.98	2.12×10^{14}
Au_2O_3	5.68	505		22.7	10.8		0.90	
$\delta = 1$ mm								
Al	4.19	390	54.5	21.2	6.9	10.2	1.34	8.18×10^{14}
Al_2O_3	6.19	712		38.8	12.3		1.16	
Au	4.78	584	26	15.2	8.4	5.1	4.93	1.07×10^{14}
Au_2O_3	5.68	762		19.8	10.8		4.60	

(a) Metals for which detailed Fowler–Nordheim plots are given at $\delta = 0.1$, 1 mm by Allan and Salim [1].
(b) Work function of the bare metal ϕ_M and corresponding oxide ϕ_{MO} from Table I.
(c) Field enhancement factor β as evaluated from iterative calculations on Equation 6 for a given ϕ_M or ϕ_{MO}, in conjunction with pre-breakdown F–N plots in [1].
(d) Observed breakdown voltage V_b at $\delta = 0.1$, 1 mm [1];
(e) Enhanced electric field at breakdown F_b from Equation 5 with values from columns (c) and (d).
(f) Field strength above which space charge effects are important, obtained from Equation 8.
(g) Breakdown current I_b extrapolated from the pre-breakdown F–N plots used for columns (c) and (h) corresponding to the V_b values of column (d).
(h) Effective cathode emitting area A evaluated from Equations 3, 4a and b with values from columns (b), (c) and the same F–N pre-breakdown plots from [1] which are used for column (b).
(i) Ratio of the value in column (g) to the root mean square of pure and oxide calculations for the same metal in column (h).

No direct, consistent data concerning j_b is available in [1]: i.e. measurements of current densities for the same electrode spacing and cathode temperature at the instant of voltage breakdown V_b for all electrode materials under study. However, F–N plots under prebreakdown conditions are provided for stainless steel, Au and Al at $\delta =$ 0.1 mm, as well as for Au and Al at $\delta = 1$ mm ([1]: Figs. 2 and 3). In Table II the breakdown currents I_b of column (g) are obtained by *extrapolating* the diagrams mentioned above to the experimentally observed breakdown voltages, V_b of column (d).

Chatterton [26] has shown that space-charge effects play an important role for field strengths above the critical value:

$$F_s = 8 \times 10^8 \phi^{3/2} \text{ V m}^{-1}. \quad (8)$$

Furthermore, Wheeler [29] has demonstrated that finite emission velocities tend to yield lower current densities than those predicted by Equation 3 for field strengths significantly below F_s. With this in mind the values of j_b in Table II, dependent as they are on F–N extrapolations for I_b and F–N calculations involving Equation 3 for effective emission areas A, can be regarded at best as upper limits to their true values at breakdown. However, for Au and Al at 300 K and gap separations $\delta \leqslant$ 1 mm, calculations show that the maximum deviation in $\ln j_b$ is:

$$\max(\Delta \ln j_b)/\overline{\ln j_b} = 7\% \quad (9)$$

with $\overline{\ln j_b}$ representing the root mean square value for the last four values of j_b in column (i), Table II. It is therefore evident that a straight line through Au_2O_3 and Al_2O_3 in Fig. 2 provides a reasonably close approximation to the dominant trend at breakdown.

The effective emitting areas A for Al and Au, calculated under pre-breakdown conditions from the F–N Equation 3, yield diameters in the range of 11 to 25 Å (Table II, column, h). This dimension is of the order of at most several lattice spacings for a purely monocrystal metal and would seem to be at variance with recent electron microscope studies [30, 31]. However, it is significant that the relative F–N dependence at breakdown of stainless steel (Fe), Nb and Cu oxides fall within ±8% of the straight line in Fig. 2. This implies that the relative values of $\ln j_b$, upon which Equation 7 depends, also differ by at most ±8%.

Although the absolute values of j_b calculated in Table II may not be realistic, Fig. 2 provides independent albeit indirect evidence that at least their relative values are preserved at breakdown. For current densities of the order $10^{14}\,A\,m^{-2}$, the condition that $\ln j_b$ varies by at most ±8% gives a range $j_b(\text{maximum})/j_b(\text{minimum}) \approx 170$. Fig. 2 confirms the validity of Equation 7, which in turn depends not only upon minor variations in $\ln j_b$, but also upon the requirement that the β for the various materials under study be similar in values at the time of breakdown. The calculated values for β in Table II are derived from pre-breakdown emission conditions.

Evidence exists that pre-breakdown electron emission is controlled by multiple protrusions possessing the highest β value and that the instability leading to breakdown can be triggered by a single high β site [1, 14, 15, 23, 26, 28, 32, 33]. Such cathode irregularities have a relatively low probability of occurrence per unit area of electrode surface [15, 30, 31]. Once breakdown has commenced, the effective β of the active emitting area can be lowered by the contribution from other, more numerous nearby protrusions with local enhanced field $F < F_b$, the field required for breakdown initiation [34, 35].

The breakdown field strengths F_b of Table II have been calculated using Equation 5, where pre-breakdown values of β are employed in conjunction with experimentally observed breakdown voltages V_b. Partial melting of dominant emission sites, due to ohmic heating and ion bombardment during the transition from pre-breakdown to breakdown conditions, will also tend to reduce the final enhancement factor β [13, 34]. The actual breakdown field strengths would then correspond to values much closer to F_s (column f, Table II) than the F_b estimated from pre-breakdown β values. Hence space charge effects may be minimized when comparing relative values of $\ln j_b$, as is done implicitly in the derivation of Fig. 2.

It is quite possible that a modified F–N plot involving work functions of the bare metals, instead of those used here for oxide-covered metals, may give a relationship similar to that of Fig. 2. The results in [1] imply that such a linear dependence can occur. Indeed, the estimated F_b for bare stainless steel (Fe at $\delta = 0.1$ mm, Table II) compares favourably with the value $(7.8 \pm 1.3) \times 10^9\,V\,m^{-1}$ derived in [14] for an assumed $\phi = 4.4$ eV, as well as with other references mentioned therein. However, the experimental conditions in [1], as well as the considerations presented in the previous sections of this article, support the presence of oxides on the electrodes, so that the work functions ϕ_{MO} of oxide-covered metals must be used.

3.2. A simplified relation

Equation 3 can be rewritten as:

$$-\ln(\phi/V_b^2) = C_1\phi^{3/2}/V_b + C_2 \qquad (10)$$

where C_1 is the slope of the straight line in Fig. 2. For the same gap separation δ and electrode temperature it is therefore essentially a constant. Variations in C_2 are dominated by differences in $\ln j_b$ for the various materials under study. These variations are of the order ±8%, as shown in the previous section, so that C_2 may also be regarded as constant for purposes of further analysis.

The upper limit of the left-hand side in Equation 10 is [36]:

$$\ln(\phi/V_b^2) \leqslant \phi/V_b^2 - 1; \quad \phi/V_b > 0, \qquad (11)$$

so that

$$\phi/V_b \geqslant \frac{(1-C_2)}{C_1\left(\dfrac{1}{C_1V_b} + \phi^{1/2}\right)}, \qquad (12)$$

where, in keeping with Equation 5, it is understood that $V_b = |V_b|$.

For polycrystalline metals of common usage [16], the work function of the bare metal is in the range

$$4.1 \leqslant \phi_M \leqslant 5.3\ (\text{eV}),$$

whereas the increase in the metal work function, due to the presence of chemisorbed oxygen [17], varies as:

$$0.4 \leqslant \Delta\phi_0 \leqslant 2\ (\text{eV}).$$

Hence the limits of the oxide-covered work function are:

$$4.1 \leqslant \phi_{MO} \leqslant 7.3\ (\text{eV})$$

so that for typical electrode metals

$$(\phi_{MO})^{1/2} \simeq 2.36 \pm 14\%. \qquad (13)$$

In addition, from Table I and Fig. 2: $(C_1V_b)^{-1} \ll 1$, which means that Equation 12 can be rewritten as:

$$\phi_{MO}/V_b \geqslant \text{constant} \pm 14\%. \qquad (14)$$

Provided $\phi_{MO}/V_b^2 > 2, \neq 0$, the inequality in Equation 11 can be relaxed to:

$$\ln(\phi_{MO}/V_b^2) = (\phi_{MO}/V_b^2 - 1)f \quad (11a)$$

where f is a function of ϕ_{MO}/V_b^2 [36]. It is therefore of interest to explore the possibility of relaxing the inequality in Equation 14 as well, i.e.

$$\phi_{MO}/V_b \sim \text{constant (eV kV}^{-1}). \quad (15)$$

Such a possibility is examined in Fig. 3 where the linear Equation 15 is seen to be roughly followed, for a gap length of 0.4 mm at 300 K.

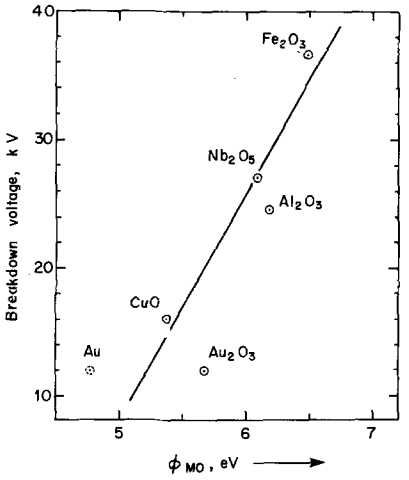

Figure 3 Breakdown voltage, V_b, for metal–vacuum–metal sandwiches composed of indicated metals versus the corresponding work function for the oxide-coated electrode at $\delta = 0.4$ mm. (Data from Table I.)

From Equations 14 and 15 there is an implied constraint

$$V_b \leqslant C_3\phi_{MO} \quad (16)$$

where, by Equations 12, 13 and 16:

$$C_3 \approx 2.36C_1/(1 - C_2). \quad (17)$$

From Figs. 2 and 3 respectively,

$$C_1 \sim 1.29, \quad C_3 \sim 17.9 \quad (18a)$$

so that by Equation 17:

$$C_2 \approx 0.83. \quad (18b)$$

Using Equations 3, 4a, b, 5 and 10 the results in Equation 18a and b translate to:

$$j_b \approx e^{0.83}\, 1.54 \times 10^{-6}\beta^2/d^2$$
$$= 3.5 \times 10^{-6}\beta^2/d^2 \,(\text{A m}^{-2}). \quad (19a)$$

For the scale of β values in Table II, Equation 19a predicts breakdown current density values, j_b, in the range:

$$\left.\begin{aligned} &\delta = 0.1\text{ mm},\ 92 < \beta < 505: \\ &\quad 3 \times 10^6 < j_b < 9 \times 10^7\,\text{A m}^{-2} \\ &\delta = 1\text{ mm},\ 390 < \beta < 762: \\ &\quad 5.4 \times 10^5 < j_b < 2.1 \times 10^6\,\text{A m}^{-2}. \end{aligned}\right\} \quad (19b)$$

The numerical relations 18a, b and 19a, b pertain only to the experimental results of Allan and Salim [1]. The estimates (19b) appear in conflict with j_b values in Table II, where the calculations are based on a strict adherence to the F–N Equation 3 and the evaluation procedures outlined in [25].

A plausible mechanism behind this apparent inconsistency has been touched upon in the previous section. Whereas the instability triggering breakdown may occur at a single high β protrusion, the affected area at breakdown may increase at breakdown with other nearby protrusions participating in the phenomenon. By regarding the I_b of Table II as the maximum total discharge current supportable by the metal–vacuum–metal sandwich, the experimentally inferred j_b values of (19b) can be used to estimate the cathode area A_b over which the breakdown phenomenon spreads, in order that such high current passage can be accommodated by the vacuum gap. In effect:

$$A_b \leqslant I_b/j_b \quad (19c)$$

where the range of j_b for a given gap separation δ comes from relations 19b and the corresponding scale of I_b is taken from Table II. The equivalent diameter D_A, of breakdown area A_b is:

$$\left.\begin{aligned} \delta &= 0.1\text{ mm} : D_A \leqslant 3.6 \times 10^{-6}\text{ m} \\ \delta &= 1\text{ mm} \ : D_A \leqslant 2.5 \times 10^{-5}\text{ m}. \end{aligned}\right\} \quad (19d)$$

It would appear more than coincidental that the D_A in (19d) are of the same magnitude as electrode microcrater formation observed by electron microscopy [4, 10, 33, 40, 45]. The calculated values of I_b in Table II cannot be regarded as being seriously overestimated, since Allan and Salim [1] use d.c. 10μA currents for conditioning the electrodes without incurring breakdown for spacings $0.1\text{ mm} \leqslant \delta \leqslant 1$ mm. Although present evidence in the literature is insufficient to pursue this aspect in greater detail, the role of electron field emission cannot be discounted as an important contributing factor

during the breakdown phenomenon itself.

As can be seen in Figs. 2 and 3, the position of oxidized stainless steel follows the trend of F–N field emission prior to breakdown, in contradiction to the semiconductivity exhibited by pure iron oxide in Fig. 1. This suggests that although the semiconducting properties related to the band gap (or heat of formation per equivalent value) may differ quite markedly for oxide-coated stainless steel, as compared with oxide-coated pure iron, the work functions of the two types of surfaces may be quite similar.

In addition, chromium oxide formation on the stainless steel surface [5, 6] is not expected to alter the results derived for Fe_2O_3 in Fig. 3. No observed or calculated values are available for an estimate of the work function ϕ_{MO} pertaining to chromium oxide. However, Equation 2 and the close correspondence of the pure Cr work function ($\phi_M = 4.40\,eV$; [16]) to that of pure Fe would imply similar values for oxide work functions.

3.3. Applicability of the simplified relation

Figs. 4 and 5 compare the experimental results of Allan and Salim [1] with breakdown voltages observed by others at two common, representative gap separations. Work functions for materials not found in Table I are presented in Table III. Only those published results have been considered for which $\delta \leqslant 1$ mm and where more than two types of electrode material have been used. The latter condition is necessary to demonstrate the linearity of V_b versus ϕ_{MO} in Equation 15.

Although much research has been done on other interesting electrode materials (such as titanium [37]), either the criteria mentioned above were not met, or the cathode material differed from that of the anode [8, 37–39]. Such a difference can result in the deposition upon the cathode surface of anode material possessing a significantly different ϕ_{MO} [40]. This would markedly change the emission properties of the cathode and render impossible the verification of Equation 15.

In both Figs. 4 and 5 it is apparent that the experimental results with least scatter are those of Denholm [10] and Maitland [11]. It is interesting to note that although Maitland's results [11] coincide with those of Allan and Salim [1] for $\delta = 0.2$ mm in Fig. 4, their slopes become markedly different for $\delta = 0.5$ mm in Fig. 5, where Maitland's [11] experimental points now tend to coincide with those of Denholm [10]. The reason for this

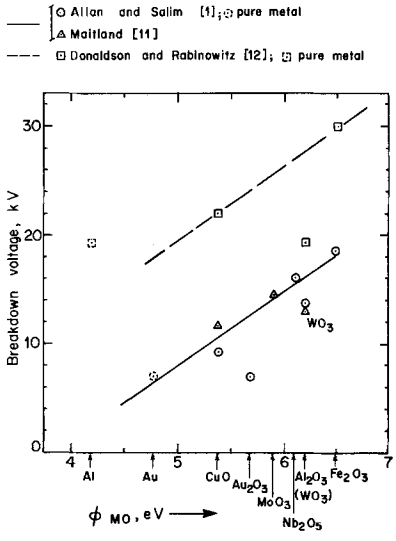

Figure 4 Test of the linear relation between breakdown voltage, V_b, and the work function of oxide-covered electrodes at $\delta = 0.2$ mm. Experimental points with common abscissa correspond to the same, unbracketed oxide material unless otherwise indicated. (Data from Tables I, III and references cited in the diagram.)

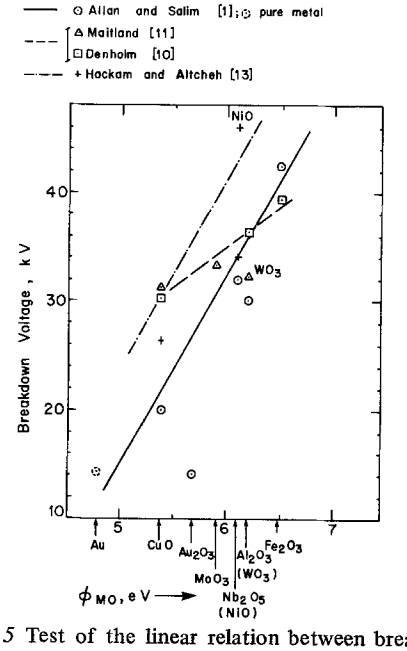

Figure 5 Test of the linear relation between breakdown voltage, V_b, and the work function of oxide-covered electrodes at $\delta = 0.5$ mm. Experimental points with common abscissa correspond to the same, unbracketed oxide material unless otherwise indicated. (Data from Tables I, III and references cited in Diagram.)

is to be found in the preparatory conditioning of the electrodes.

Maitland [11] prepares his electrodes by 2000 to 3000 breakdown pulses at each setting before proceeding to a final determination of the break-

TABLE III Work functions and melting temperatures of electrode materials appearing in Figs. 4 and 5. Symbols and references are as defined in Table I

Metal	ϕ_M (eV)	$\Delta\phi_0$ (eV)	ϕ_{MO} (eV)	T_{MO} (°C)	T_M (°C)
Mo	4.30	1.6	5.9	795	2620
W	4.55	1.6	6.2	1472	3370
Ni	4.73	1.4	6.1	1957	1455
Ti	4.1	–	–	1855	1800
Cr	4.40	–	–	2437	1890

down voltage V_b. This procedure tends to blunt, partially destroy or melt dominant surface protrusions to the extent that a lower cathodic β value is achieved than for an otherwise untreated surface. As can be seen in Equation 5, lower β values necessitate higher applied voltages V_b to reach the critical field strength F_b required for breakdown initiation. Denholm [10] obtains much the same results with a preparatory d.c. discharge of 3 min duration, in 10 Torr hydrogen, at currents between 1 A for stainless steel to 0.25 A for aluminium.

As seen in Fig. 4, the passage of a 30 min long, pre-breakdown current of 10 μA d.c. at a nominal 10^{-7} Torr by Allan and Salim [1] gives a trend similar to that of Maitland [11], and possibly Denholm [10] as well, for $\delta = 0.2$ mm [13]. However, these three different conditioning procedures may not all be as equally effective at larger $\delta \sim$ 0.5 mm, possibly due to beam spreading [37]. This disparity would account for the different slopes apparent in Fig. 5.

Further evidence of non-uniform results attributable to a chosen conditioning process for different materials is provided by Hackam and Altcheh [13]. Since the aim of this particular experiment is to compare the effect of air pressure on V_b with those at UHV (10^{-9} Torr), heating of the electrodes during the conditioning process is deliberately avoided. Since Ni and Nb possess the same ϕ_{MO} as well as similar oxide melting temperatures (Tables I and III), the reason for the wide divergence in their breakdown voltages in Fig. 5 must be sought elsewhere. A highly probable explanation can be found in the vastly different melting points of protrusions in the pure Ni or Nb substrate upon which a relatively thin oxide film may form. The highly refractory Nb would be much more resistant to changes in its surface structure during the conditioning process than would Ni. More high β emission sites tend to remain on the Nb surface and hence the trend towards lower breakdown voltage V_b [13]. The same interpretation can be advanced for the case of tungsten electrodes in Figs. 4 and 5.

On the other hand, the proclivity of aluminium electrodes towards relatively low V_b values in Figs. 4 and 5 can be attributed to the high melting point of aluminium oxide. As has been demonstrated in Sections 1 and 3.2, it is not necessary that the entire electrode surface be wholly covered by oxide film. The existence of a small, localized area of oxide on the aluminium electrode surface would favour the formation of isolated cathodic irregularities, even in circumstances of severe conditioning or breakdown: either by erosion and/or gradual melting of the surrounding pure metallic surface, or by explosive Joule heating of the oxide [34].

This general deviation of aluminium electrodes from the major trends of Figs. 4 and 5 is accentuated with the overall higher V_b values observed by Donaldson and Rabinowtiz [12]. Whereas the V_b in all other references were observed under essentially stable d.c. conditions at pressures less than 10^{-5} Torr, the applied voltage in [12] rose at a rate of 3 kV sec^{-1} at a nominal base pressure 10^{-5} Torr. Higher V_b values are to be expected with this combination of a dynamic, as opposed to d.c. charging procedure [10, 13] and a transition pressure regime $\geqslant 10^{-5}$ Torr [13]. Nevertheless, a characteristic line through experimental points [12] can be drawn with slope similar to that of other experiments at $\delta = 0.2$ mm (Fig. 4).

The coincidence of V_b for pure Au rather than Au_2O_3 in Fig. 4 supports the hypothesis, in Section 2, that the contribution of gold oxide to gap potentials can be neglected at small spacings ($\delta \leqslant 0.2$ mm). Higher V_b values than expected for Au electrodes in Figs. 3 and 5 are possibly due to more energetic pre-breakdown conditions across larger gaps ($\delta > 0.2$mm). Higher mean fields E and pre-breakdown currents could effectively reduce the β value of the emitting surface.

Figs. 3 to 5 lend general credence to Equation 15, which is based on a comparison of relative breakdown characteristics for several materials. In this relative sense, F–N emission conditions can be valid even at or very near breakdown, despite the possibility that the absolute behaviour of an individual metal–vacuum–metal sandwich may exhibit significant deviation due to space charge or other effects [26, 29]. Since F–N emission conditions are valid up to 450 K [4], a possible application of Equation 15 might be the estimate of

breakdown voltage, V_b, for a wide variety of oxide-coated polycrystalline metals of common usage and known ϕ_{mO} values [16, 17]. The linear relation in Figs. 3 to 5 implies that such a method involves the precise knowledge of V_b versus ϕ_{MO} for only two metals possessing significantly different metal–oxide work functions at a given temperature, in the range 4.2 to 450 K, and fixed gap conditions $\beta, \delta < 1$ mm.

Deviations from the general linear trend of Equation 15 can be explained to a great extent in terms of differing field intensification factors β. In this context Equation 15, together with some knowledge of the heat properties of the metals and their oxides (e.g. melting point, heat capacity, etc.), may also be used to sort out the effects of intrinsic emission properties from those due to surface structure [23]. An example of this type of problem is the discussion in this section on observations by Hackam and Altcheh [13] of breakdown in Nb and Ni gaps. In effect, then, Equation 15 can serve as a means to evaluate the efficacity of the conditioning process on different types of metal–vacuum–metal sandwiches, where the involvement of oxides is suspected.

4. Estimate of the oxide layer thickness

The functional dependence of the d.c. breakdown voltage $V_b(M)$, (in kV, for a particular electrode material M), on the gap separation δ (in mm) is observed to be:

$$V_b(M) = k_1(M)\,\delta^{\alpha(M)} + k_2(M). \qquad (20)$$

For short δ (generally < 1 mm), $k_1(M)$ is a constant particular to the electrode surface material and experimental conditions, $\alpha(M) \sim 1$ [41–43] and $k_2(M)$ is determined by the minimum value of δ for which Equation 20 is observed to hold true [13]. The right-hand side of Equation 20 is given in Table IV for various materials, as observed by Allan and Salim [1]. In general, for $\delta > 1$ mm, $k_1(M)$ and $k_2(M)$ assume different constant values and $\alpha(M) < 1$ [1, 44–46].

The properties of Au electrodes for $\delta < 0.2$ mm can be used in conjunction with equations 5 and 20 to estimate an effective oxide layer thickness that is consistent with the correlations of Sections 2 and 3. The method is to equate the V_b dependence in Equation 20 for Au with that of the metal(M)–vacuum–metal(M) sandwich under consideration and to solve for the common electrode distance δ_0 at which the same breakdown voltage V_b occurs. Each such case represents the minimum gap separation $\delta_0 > 0$ for which Equation 20 holds true experimentally. The condition $\delta \sim \delta_0$ can also be regarded as representative of the transition regime in which the coefficients of Equation 20 must undergo change for gap separations $0 \leqslant \delta < \delta_0$: a range not easily amenable to present methods of measurement. It is in this transition regime that a re-interpretation of the V_b versus δ dependence in Equation 20 can be postulated, which must of necessity include a correspondence between the breakdown voltage for gap separations $0 \leqslant \delta < \delta_0$ and those observed for $\delta \sim 0.1$ mm.

The first step in the estimation procedure is to solve

$$V_b(\mathrm{Au}, \delta_0) = V_b(\mathrm{M}, \delta_0) \qquad (21)$$

for δ_0 by iteration, using Equation 20:

$$k_1(\mathrm{Au})\,\delta_0^{\alpha(\mathrm{Au})} + k_2(\mathrm{Au}) = k_1(\mathrm{M})\,\delta_0^{\alpha(\mathrm{M})} + k_2(\mathrm{M}) \qquad (22)$$

with values for α, k_1, k_2 as listed in Table IV.

Since the oxide of Au can be regarded as either non-existent (Fig. 3) or highly conducting (Section 2), one would expect the contact voltage to be much less than $k_2(\mathrm{Au}) = 1.36 \times 10^3$ V as listed in

TABLE IV Parameters used in calculations of the effective oxide layer thickness.

(a) Metal (M)	(b) $V_b(M, \delta)$ (kV)	(c) δ_0 (mm)	(d) X_{MO} (V m^{-1})	(e) ω_{MO} (Å)
Au	$23.83\,\delta^{0.88} + 1.36$	–	–	–
Fe (Stainless steel)	$81.4\,\delta^{0.83} - 1.54$	2.5×10^{-2}	$2 \times 10^{}$	144
Nb	$52.5\,\delta^{0.77} + 1.089$	1.47×10^{-3}	4.65×10^{8}	88
Al	$51.87\,\delta^{0.8} - 0.421$	2.5×10^{-2}	7.9×10^{8}	37

(a) Gold and metals for which the oxide field strength X_{MO} is known.
(b) Functional dependence, Equation 20, of breakdown voltage V_b on gap separation for $\delta \leqslant 1$ mm as observed in [1].
(c) Gap separation satisfying Equation 22.
(d) Maximum field strength sustainable across a smooth film of the corresponding oxide [48, 49].
(e) Effective oxide layer thickness calculated from Equations 26 and 28 and column (d).

Table IV [15]. This would lead to an expectation that a different dependence of V_b on δ exists, for Au at least, in the range $0 \leqslant \delta \ll 0.1$ mm. Such a change would be analogous with transitions on the scale $0.1\text{ mm} \leqslant \delta \leqslant 1$ mm as observed in [13, 47]. The requirement for such a transition in the regime $\delta \to 0$ is apparent in the relative values of k_2(M) in Table IV. In the notation of Equation 20, the functional relation must become for Au

$$V_b(\text{Au}, \delta) = k_1(\text{Au})\delta^{\alpha(\text{Au})}, \quad \delta < \delta_0 \quad (23)$$

where k_1(Au), α(Au) would have values different for those of Au in Table IV. The transition for Au from the Equations 20 to 23 in the vicinity δ_0 leads to a re-interpretation of Equations 21 and 22, which can be formulated as:

$$k_1(\text{Au})\delta^{\alpha(\text{Au})} + V_{MO} = V_b(\text{M}), \quad \delta \leqslant \delta_0 \quad (24)$$

i.e. the Au–vacuum–Au sandwich equivalent in V_b and δ_0 to the M–vacuum–M sandwich under investigation, can be regarded as a calibrating gap with electrodes covered by an effective layer of oxide for the corresponding electrode material M. Consequently:

$$k_2(\text{Au}) = V_{MO} = \beta^* X_{MO}\omega_{MO}. \quad (25)$$

Here, X_{MO} is the maximum field strength sustainable by a smooth oxide film (Table IV), ω_{MO} is the film thickness and β^* is the effective field intensification factor for the oxide corresponding to the electrode material M. The oxide layer characterized by Equation 25 is to be regarded as a film deposited on the gold substrate of the Au–vacuum–Au gap.

The constant $k_2(\text{Au}) = 1.36 \times 10^3$ V now assumes the role of the oxide contribution to the Au gap potential. Field strengths X_{MO} for oxide films on Al and Nb [48] and on Fe [49] are obtainable from the literature dealing with anodic (electrolytic) oxide growth on metals. Unfortunately, similar data are not available for the oxides of Au and Cu.

Equation 25 may be rewritten, so that in terms of the experimental observations of Allan and Salim [1], the effective oxide film thickness ω_{MO} can be estimated as:

$$\omega_{MO} = k_2(\text{Au})[\beta^* X_{MO}]^{-1} = 1.36 \times 10^3 [\beta^* X_{MO}]^{-1}. \quad (26)$$

The field enhancement factor β^*, which corresponds to the gap separation δ_0 of Equation 22, remains to be determined. As noted in Sections 1 and 3.1, the critical area for oxide deposition involves only those microprotrusions that dominate the pre-breakdown history of the gap, so that the oxide layer need not be deposited over the entire electrode surface. The calculation has been reduced to a consideration of the effects induced by an oxide coating on a gold substrate. The enhancement factor β^* would therefore be quite high, in keeping with sudden breaks of the oxide layer which is spotted over the surface of the "equivalent" gold electrode. However, the surface condition of the underlying gold substrate will determine to a large extent the magnitude of β^*. If it is assumed that the thickness of the effective oxide coating in the equivalent Au–vacuum–Au gap is much less than the height of microprotrusions on the gold surface, then:

$$\beta^* \simeq \beta(\text{Au}, \delta_0). \quad (27)$$

The right hand side of Equation 27 may be evaluated by using Equation 5 and the experimentally verifiable fact that the enhanced critical breakdown field F_b remains constant for the same electrode material in gaps where $\delta \leqslant 1$ mm [13–15]. Table II shows this to hold true for gold, albeit the calculated F_b is much higher than the value $(7.8 \pm 1.3) \times 10^9\,\text{V m}^{-1}$ accepted for other materials [14]. The great difference in F_b for Al, Al_2O_3 for the gap separations $\delta = 0.1$, 1 mm in Table II can be attributed to a rapid change of coefficients in Equation 20 over $0.1 \leqslant \delta \leqslant 1$ mm as opposed to a more gradual transition for Au [1]. This constancy in F_b for Au lends further support to the use of Equation 24, i.e. an "equivalent" oxide coated Au–vacuum–Au sandwich, for estimates of the oxide layer thickness.

The required enhancement factor β^* is extrapolated from experimentally determined parameters at $\delta = 0.1$ mm for Au electrodes. Using Equation 5 in conjunction with Equations 23 to 25 and 27,

$$\beta^* = \beta(\text{Au}, \delta_0) = [F_b(\text{Au}, \delta = 0.1\text{ mm}) \times d_0][V_b(\text{M}, \delta_0) - k_1(\text{Au})]^{-1} = 17.4 \times 10^9 d_0 [V_b(\text{M}, \delta_0) - 1.36 \times 10^3]^{-1}. \quad (28)$$

Here $d_0 = \delta_0 \times 10^{-3}$ m, F_b(Au, $\delta = 0.1$ mm) comes from Table III. whereas the value of k_2(Au)

defined in Equation 22 is found in Table IV. $V_b(M, \delta_0)$ is the common voltage which determines the gap separation δ_0 common to both the M–vacuum–M gap and the corresponding gold sandwich, as expressed in Equation 22. $V_b(M, \delta_0)$ can be calculated from the data supplied in Table IV.

Equations 26 and 28 yield an estimate of the oxide layer thickness ω_{MO} for a given metal–vacuum–metal gap (column e, Table IV), which is consistent with the correlations in Sections 2, 3 and with the functional Equation 20. Although these calculations are based on the model of an equivalent, oxide-covered gold sandwich, the result agrees well with observations of naturally occurring oxide film on aluminium (20 to 40 Å at standard pressure and 300 K [50]). In the case of iron oxide on a stainless steel surface (Fe of Table IV), $\omega_{Fe_2O_3}$ is 3 to 5 times greater than the equilibrium oxide layer observed at atmospheric pressure and room temperature by ellipsometric studies ($\omega_{MO} \sim 50$ Å [31], ~ 30 Å [6, 50]). Fane *et al.* [6] point out that the formation of chromium oxides in lieu of those pertaining to iron on a stainless steel surface would result in only a 10% observable difference.

Since independent measurements for the equilibrium thickness of oxide film on Nb are not readily available, a further comparison of the estimated ω_{MO} can be pursued with confidence only in the case of stainless steel and aluminium vacuum gaps. Additional support for such a comparison comes from the common δ_0, and therefore the same "transitional" breakdown voltage $V_b(M, \delta_0)$ of Equation 21, for the latter two types of sandwich.

It must be remembered that the ω_{MO} of Equation 26 are only rough estimates. However the conformity of the calculated $\omega_{Al_2O_3}$ with the independent measurements cited above leads naturally to the possibility that a thicker oxide film can be formed on a stainless steel surface than that on Al for similar applied voltages. Confirmation of such a tendency can be seen in the different melting temperatures for the oxides of Fe and Al (Table I).

During preconditioning and/or breakdown, the temperature near the emitting area of the electrode may be sufficiently high to allow Fe oxide formation and deposition at faster rates than for the oxides of Al, which require relatively higher temperatures of formation. Moreover, due to high local temperatures within the gap during the emission process, the dynamic balance between the generation of electrode vapour and the eventual deposition of oxide on the cathode surface can proceed at rates greater than that characteristic of equilibrium film formation at atmospheric pressure and 300 K. The observations of Allan and Salim [1] favour such a model, since cooling of the cathode (4.2, 77.3 K as opposed to an anode temperature maintained at 300 K) would increase the surface-to-vapour temperature difference and hence the rate of condensation of metallic and oxide vapour on the electron emitting surface. Thicker oxide films at these lower temperatures lead to the uniformly higher V_b values observed for the same δ.

Allan and Salim [1] state that oxide film is present on all electrode materials tested except gold. However, no reference is made to an independent identification procedure of these contamination layers. Observed reductions in pre-breakdown current are attributed in part to the certain presence of residual and adsorbed gases and their possible condensation on the cold cathode surface. Hackam and Raju [47] have explored the influence of various types of residual gases on the breakdown voltage in Equation 20 at 7×10^{-7} Torr. In particular, the occurrence of oxide film on aluminium reduces the reflectivity of the electrode surface to an increased extent in the visible region of the radiation spectrum [50]. Should the oxide film possess light absorbing properties as well, the presence of localized areas of oxide layers on the electrode surface may be detectable by eye. Denholm [10] has noted higher insulation strengths for "dull" aluminium electrodes as opposed to those with a "bright" finish.

5. Conclusion

It is apparent that the presence of oxides can have a marked effect on the magnitude of breakdown voltage during dielectric breakdown of metal–vacuum–metal sandwiches. Correlation tests should be employed to determine whether oxide layer formation plays a significant role in the experimental results. It is highly probable that the work function of the electrode surface will require the contribution from a corresponding oxide layer, if a valid analysis of the data is to be made.

A source of contaminating oxide has been associated with desorption from the walls of the confining vessel as well as from the electrodes [7]. This, coupled with the presence of even minute traces of oxygen in the gap during the conditioning

procedure can lead to elevated oxide deposition rates on dominant emission sites. Experimental evidence [1], in conjunction with theoretical considerations [26, 44], shows that the pre-breakdown current can be explained by a cold-cathode field emission process. The breakdown mechanism itself can be considered as arising from an instability at either the anode or cathode, which is triggered by the field emission of electrons from the cathode sites. The damage to cathode microprotrusions upon breakdown [13], together with a comparison of melting susceptibilities for oxides in Section 4, favours the occurrence of this critical instability at the cathode surface.

A detailed description of the critical breakdown phenomena is beyond the scope of this article. Ridley [34] explores the oxide role in such a theory, albeit in the specialized case for SiO_2 films. Nevertheless, the oxide influence upon Fowler–Nordheim injection from a cathode protruberance, the oxide effect on Joule heating and explosion of the protruding filament, and the contribution of oxides to mobile positive ions which enhance the injecting field (either from within the solid electrode or the gap itself) will manifest themselves, of necessity, in correlation effects similar to those discussed in this article.

Acknowledgements

The support of the National Research Council of Canada under grant No. A6373 and of the Hydro-Quebec Research Institute (Varennes) is gratefully appreciated.

References

1. R. N. ALLAN and A. J. SALIM, *J. Phys. D: Appl. Phys.* 7 (1974) 1159.
2. R. GOMER, "Field emission and field ionization" (Harvard University Press, 1961) pp. 30–31, 47.
2a. *Idem, ibid,* pp. 6–9
3. A. J. T. HOLMES, *J. Phys. D: Appl. Phys.* 7 (1974) 1412.
4. C. S. WALTERS, M. W. FOX and R. V. LATHAM, *ibid* 7 (1974) 911.
5. R. V. LATHAM, *ibid* 5 (1972) 2044.
6. R. W. FANE, W. E. J. NEAL and R. V. LATHAM, *J. Appl. Phys.* 44 (1973) 740.
7. G. P. BEUKEMA, *J. Phys. D: Appl. Phys.* 6 (1973) 1455.
8. N. B. ROSANOVA and V. L. GRANOVSKII, *Sov. Phys. – Tech. Phys.* 1 (1956) 471.
9. D. L. ADAMS and L. H. GERMER, *Surface Sci.* 32 (1972) 205.
10. A. S. DENHOLM, *Can. J. Phys.* 36 (1958) 476.
11. A. MAITLAND, *Brit. J. Appl. Phys.* 13 (1962) 122.
12. E. E. DONALDSON and M. RABINOWITZ, *J. Appl. Phys.* 34 (1963) 319.
13. R. HACKAM and L. ALTCHEH, *ibid* 46 (1975) 627.
14. R. HACKAM and S. K. SALMAN, *ibid* 45 (1974) 4384.
15. D. ALPERT, D. A. LEE, E. M. LYMAN and H. E. TOMASHKE, *J. Vac. Sci. Tech.* 1 (1964) 35.
16. S. TRASATTI, *J. Chem. Soc. Farad. Trans. I* 68 (1972) 229.
17. O. JOHNSON, *J. Res. Inst. Catalysis* 19 (1971) 152.
18. A. K. VIJH, "Electrochemistry of metals and semiconductors" (Marcel Dekker, New York, 1973) Ch. 5.
19. *Idem,* "Oxides and oxide films", Vol. 2, edited by J. W. Diggle (Marcel Dekker, New York, 1973) Ch. 1.
20. R. L. PARK, J. F. HOUSTON and D. G. SCHEINER, *J. Vac. Sci. Tech.* 9 (1972) 1023.
21. R. T. SANDERSON, "Chemical periodicity" (Reinhold, New York, 1960).
22. *Idem,* "Inorganic chemistry" (Reinhold, New York, 1967).
23. D. W. WILLIAMS and W. T. WILLIAMS, *J. Phys. D: Appl. Phys.* 7 (1974) 1173.
24. R. GOMER, *Acct. Chem. Res.* 5 (1972) 41.
25. R. H. GOOD, JUN. and E. W. MÜLLER, "Handbuch der Physik" Vol. 21 (Springer-Verlag, Berlin, 1965) p. 176.
26. P. A. CHATTERTON, *Proc. Phys. Soc.* 88 (1961) 231
27. R. E. BURGESS, H. KROEMER and J. M. HOUSTON *Phys. Rev.* 90 (1953) 515.
28. G. E. VIBRANS, *J. Appl. Phys.* 35 (1964) 2855.
29. C. B. WHEELER, *J. Phys. A.* 6 (1973) 1439.
30. R. HACKAM, *J. Appl. Phys.* 45 (1974) 114.
31. R. V. LATHAM and E. BRAUN, *J. Phys. D: Appl. Phys.* 3 (1970) 1663.
32. K. F. POOLE and A. VENEMA, "Proceedings of the 4th International Vacuum Congress, Manchester" (London: IPPS, 1968) p. 271.
33. I. BRODIE, *J. Appl. Phys.* 35 (1963) 2324.
34. B. K. RIDLEY, *ibid* 46 (1975) 998.
35. T. J. LEWIS, *ibid* 26 (1955) 1405.
36. R. ZUCKER, "Handbook of mathematical functions", Applied Math. Series No. 55, edited by M. Abramowitz and I. A. Stegun (National Bureau of Standards, U.S. Govt. Printing Office, Washington D.C., 1970) p. 68.
37. G. P. BEUKEMA, *J. Phys. D: Appl. Phys.* 7 (1974) 1740.
38. I. N. SLIVKOV, *Sov. Phys. – Tech. Phys.* 2 (1957) 1928.
39. P. I. BIRADAR and P. A. CHATTERTON, *J. Phys. D: Appl. Phys.* 3 (1970) 1653.
40. G. A. FARALL, M. OWENS and F. G. HUDDA, *J. Appl. Phys.* 46 (1975) 610.
41. R. HAWLEY and A. A. ZAKY, *Prog. Dielectri.* 7 (1967) 115.
42. R. HAWLEY, A. A. ZAKY and Z. M. E. ELDINE, *Proc. IEE* 112 (1965) 1237.
43. R. HACKAM and S. K. SALMAN, *ibid,* 119 (1972) 1747.
44. A. MAITLAND, *J. Appl. Phys.* 32 (1961) 2399.
45. R. HAWLEY, *Nature, Lond.* 199 (1963) 978.

46. H. C. MILLER, *Phys. Letters,* **12** (1964) 184.
47. R. HACKMAN and G. R. G. RAJU, *J. Appl. Phys.* **45** (1974) 4784.
48. A. K. VIJH, *J. Electrochem. Soc.* **116** (1969) 972.
49. D. A. VERMILYEA, "Advances in Electrochemistry and Electrochemical Engineering", Vol. 3, edited by P. Delahay (Interscience, New York, 1963).
50. H. E. BENNETT and J. M. BENNETT, "Physics of Thin Films", edited by G. Hass and R. E. Thun, "Advances in Research and Development", Vol. 4 (Academic Press, New York, 1967) p. 37–41.
51. "Handbook of Chemistry and Physics", 41st Edn. (Chemical Rubber Publishing Co, Cleveland, Ohio, 1959).

Received 5 November 1974 and accepted 12 May 1975.